metals

MDPI

Article

Wear and Rolling Contact Fatigue Analysis of AISI 52100 Bearing Steel in Presence of Additivated Lubricants

Shubrajit Bhaumik [1,2] and Viorel Paleu [3,*]

[1] Wagner High Quality Lubricants, Chennai 603202, India; shubrajit.bhaumik@wagner-german-oil.com
[2] Tribology and Surface Interaction Research Laboratory, Department of Mechanical Engineering, SRM Institute of Science and Technology, Kattankulathur 603203, India
[3] Machine Design, Mechatronics & Robotics Department, Mechanical Engineering Faculty, Gheorghe Asachi Technical University of Iasi, 700050 Iasi, Romania
* Correspondence: vpaleu@mec.tuiasi.ro

Abstract: Tribological properties of lithium potassium titanate (PT), molybdenum disulphide, and tungsten disulphide-dispersed mineral oil (MO) were investigated. The sample containing 2 wt.% WS_2 exhibited the lowest coefficient of friction. However, the wear scar diameters of the additivated samples were very narrow. Extreme pressure properties of mineral oil were enhanced with the addition of additives. The rolling contact fatigue results exhibited better fatigue life of the balls in MoS_2 and PT-dispersed MO. Surface characterization of the balls indicated more pitting on the balls of the MO and WS_2-dispersed MO as compared to MoS_2 and PT, indicating a stable film in the case of MoS_2 and PT, which was confirmed by the presence of additives on ball surfaces by Raman spectrograph. The results of extended rolling contact fatigue tests proved that PT-added mineral oil provided the highest life cycles of the tested balls, followed by MoS_2 and WS_2-added mineral oil; thus, indicating PT as a plausible alternative to MoS_2 and WS_2.

Keywords: lithium potassium titanate; molybdenum disulphide; tungsten disulphide; anti-wear; extreme pressure; rolling contact fatigue

Citation: Bhaumik, S.; Paleu, V. Wear and Rolling Contact Fatigue Analysis of AISI 52100 Bearing Steel in Presence of Additivated Lubricants. *Metals* **2021**, *11*, 907. https://doi.org/10.3390/met11060907

Academic Editor: Zhengyi Jiang

Received: 13 May 2021
Accepted: 31 May 2021
Published: 2 June 2021

1. Introduction

Lubrication is an important practice in any process industry and selecting the right lubricant with proper additives is an important task for any maintenance engineer. Lubricants form the heart of the machineries as they help in reducing the friction between the mating pairs. Mineral oils derived from fossils are the most widely used lubricants in industries, till date. Various researchers have studied the tribological properties of these mineral oils as lubricants and have recommended the usage of several additives to enhance their performances [1,2]. Thus, the mineral oils further act as carriers for these additives [3]. The commercial mineral oils available in the markets consist of about 90–95% of base mineral oil and 5–10% of additives. With the demand for high-performance lubricants with enhanced tribological properties, the tribological properties of tungsten disulphide (WS_2) [4,5] and molybdenum disulphide (MoS_2) were investigated [6], which have been considered as efficient emergency extreme pressure solid lubricants in industries. The formation of a stable lubricant film by MoS_2 and other sulphates is the major reason for combating friction and wear [7]. Charoo et al. [8] dispersed MoS_2 of 3 µm, 5 µm, 7 µm, and 90 nm in SAE 20W40 and evaluated the tribological properties of the lubricant between EN 31 and AISI 52100 tribo-pair at 75 N, 100 N, and 125 N. The wear scar diameters in MoS_2-dispersed lubricants were almost 20% smaller than the wear scar diameters exhibited by the lubricant without MoS_2. Additionally, it was also reported that the smaller the MoS_2 size, the better are the tribological properties. Saidi et al. [9] synthesized hydrophobic MoS_2 submicro particles and dispersed them in poly-alpha-olefin (PAO) oils and reported a low frictional coefficient of about 0.02, indicating the role of dispersants in a

lubricant in controlling friction. The enhancement of tribological properties also depends on the morphology of the additives used in the lubricants [10,11]. Vaitkunaite et al. [12] dispersed molybdenum dithiocarbamate (MoDTC) in low viscosity oil and reported the decomposition of MoDTC to MoS_2 to be the primary reason in enhancing the tribological properties of the oil. Similar to molybdenum disulphide, tungsten disulphide used as a lubricant additive also enhanced the tribological properties of lubricants. An et al. [13] used nano lamellar tungsten disulphide and molybdenum disulphide as additives in oil based lubricants (M8V) and reported enhanced tribological properties of the lubricant. Additionally, it was also reported that the lamellar structure of the additives is an important factor responsible for the enhancement of the tribological properties of the lubricant.

To the best knowledge of the investigators, there has been no work reported on the tribological properties of lithium potassium titanate particles dispersed lubricants; thus, comparing the test results with commonly used additives, such as tungsten disulphide and molybdenum disulphide, would pave new ways for enhancing the tribological properties of lubricants. In an attempt to propose new performant additives for mineral oils, the present work investigates the tribological properties of tungsten disulphide and molybdenum disulphide micro particles dispersed in mineral oil, comparing them against a mineral oil blended with lithium potassium titanate micro particles. The anti-wear, extreme pressure, and rolling contact fatigue resistance properties of lithium potassium titanate, tungsten disulphide and molybdenum disulphide-dispersed mineral oils are investigated, drawing a clear conclusion about the performance of the mineral oils blended with these additives.

To our knowledge, not much research has been conducted on these additives. Therefore, our research on tribological performance and rolling contact fatigue (RCF) of AISI 52100 balls lubricated by lithium potassium titanate (PT), molybdenum disulphide (MoS2), and tungsten disulphide (WS2)-dispersed mineral oils is a novelty.

2. Materials and Experimental Methods

2.1. Preparation of the Lubricant

Commercial mineral oil (220 cSt) (MO) was used in this work. Lithium Potassium titanate (PT) (2–5 μm), molybdenum disulphide (MoS_2) (4.9 μm) and tungsten disulphide (WS_2) (9 μm) (supplied by M/s Alroko GmBh, Germany and M/s Otsuka Chemical Co., Ltd., Osaka, Japan) were dispersed in MO in various weight percentages (0.1, 0.5, 1.0, 2.0, 3.0, 4.0, and 5.0). The molecular formula of lithium potassium titanate powder is K0.80 Ti1.733 Li0.267 O4. The dispersion was first stirred for one hour using a magnetic stirrer (Model: 2MLH, REMI, Chennai, India), and then sonicated for 45 min using a probe sonicator (Make: Ultra Autosonic, Pune, India). The sonication was performed intermittently in order to avoid heating of the dispersions. Since no dispersants were used, the dispersions were immediately used for various testing.

In order to understand the purity of the additives, the additives were characterized using a micro Raman spectrograph (Make: HORIBA, Longjumeau, France; Model: LabRAM HR Evolution). Figure 1 shows the characteristic Raman spectra of the additives used in this work. The reported values of Raman spectra of tungsten disulphide and molybdenum disulphide are quite close to those reported in other works [14,15]. However, very limited reported results on lithium potassium titanates could be traced, so the reported Raman spectra of PT was seen very close to potassium titanates [16] and lithium titanates [17], indicating the purity of the additives used in the work.

Further investigations carried out for the optimization of the additivated mineral oil were planned according to Figure 2.

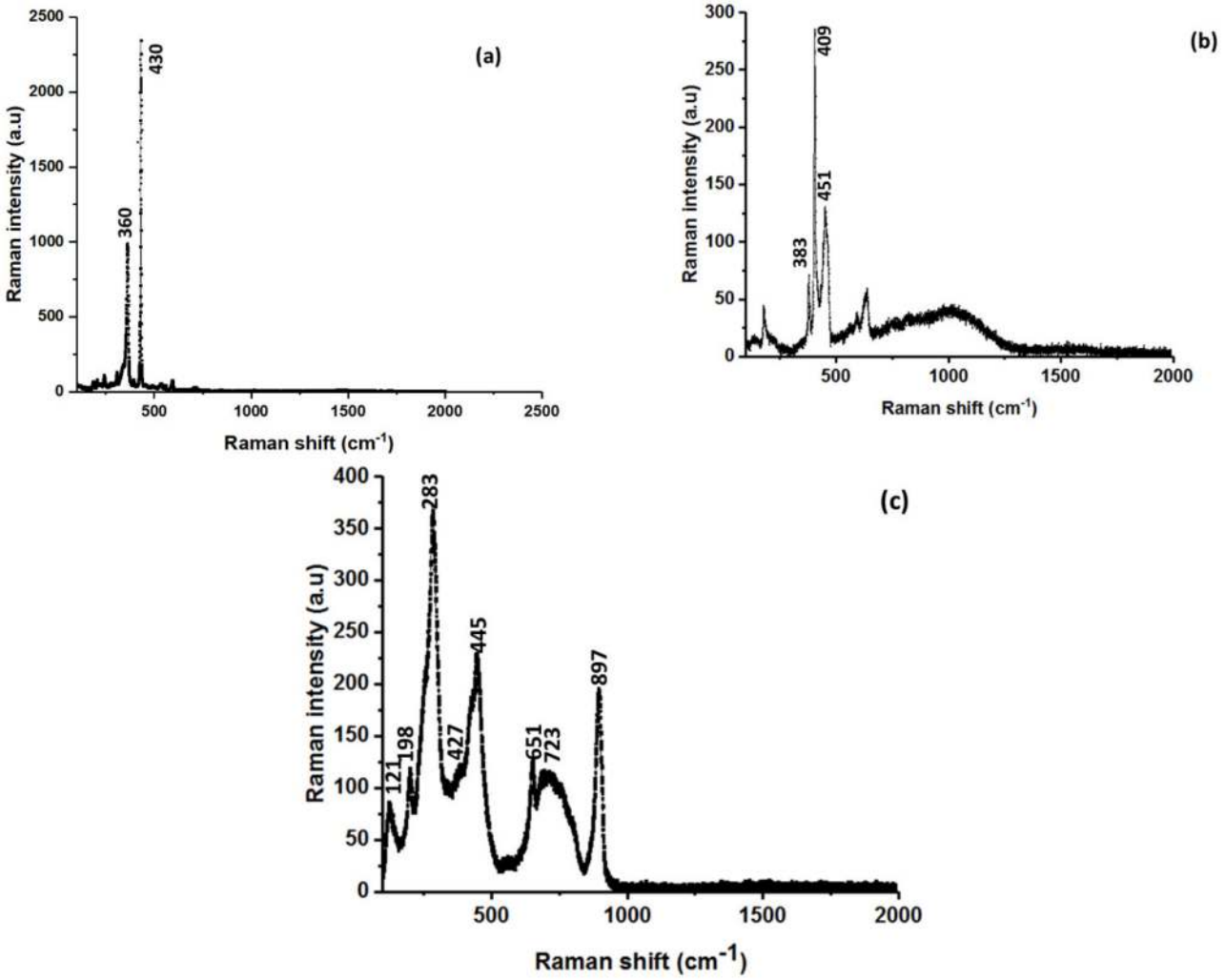

Figure 1. (**a**) Raman spectra of WS_2; (**b**) Raman spectra of MoS_2 (383, 409 cm^{-1}) (Mo1); (**c**) Raman spectra of PT.

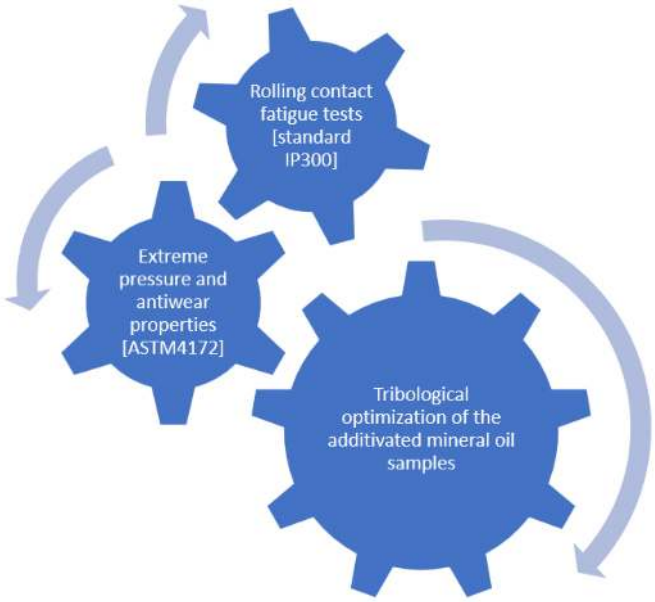

Figure 2. Research development plan.

2.2. Investigating the Anti-Wear (AW) and Extreme Pressure (EP) Properties of the Lubricants

The anti-wear properties of the lubricant samples were investigated using a four-ball tribometer following the ASTM 4172 standards [18]. The four-ball machine is from TR30 series (Model number: TR 301; Software: WINDUCOM; Make: DUCOM, Bengaluru, India). Three steel balls (AISI 52100; hardness 58–60 Rc) were fixed stationary in the ball pot and the fourth ball was rotating at 1200 rpm. A normal load of 392N was applied and the tests ran for 3600 s. The oil temperature was maintained at 75 °C using a thermocouple. The anti-wear tests were repeated thrice for each sample and an average of the coefficient of friction was reported. The extreme pressure properties of the lubricant samples (with lowest coefficient of friction) were investigated according to ASTM 2783 [19]. Each test ran for 10 s and loads were applied till all of the four balls were welded. Similar to the anti-wear test, the ball pot contained three stationary balls and the fourth ball rotated at 1760 rpm.

2.3. Investigating the Rolling Contact Fatigue Resistant Properties of the Lubricants

The rolling contact fatigue of the AISI 52100 balls exhibiting the least coefficient of friction in the presence of the tested lubricants was evaluated using the four-ball tribometer as per the IP 300 standard. Unlike the AW and EP tests, the balls in the ball pot were not fixed and stationary. A special type of ball pot was used with races for the lower balls, allowing them to rotate and revolve during the tests. The fourth ball was rotated at 1450 rpm. A load of 391 N was initially applied for 30 s and after that, the load was gradually increased until any of the balls failed by pitting. The appearance of pitting on the surface of any of the balls was detected by an accelerometer which was connected to a data acquisition system. As soon as the accelerometer picks up the change in vibrations level, it will send the signal to a dedicated software interface for pitting detection which shuts down the four-ball tribometer by the mean of the analogue output channel of the data acquisition system and stops the counter of cycles at which the pitting occurred. The occurrence of pitting on balls was confirmed by optical microscopy analysis. Ten tests were repeated for each sample, and the results were plotted as discussed in a later section. The standard lives of the balls L_{10}, L_{50} and L_{90} were determined from the Weibull plots, as shown in [20].

2.4. Measuring the Physico-Chemical Properties of the Lubricants

For viscosity measurements, a Redwood Viscometer was used. This viscometer is suited for viscosity measurements of petroleum-based products, being used for observing the effect of temperature on viscosity. According to the catalogue, its accuracy is $+/-3$ °C and readability is $+/-0.5$ °C.

The viscosity of the lubricants was measured at 40 °C and 100 °C, as per the ASTM standards (Table 1). It can be seen that the blending with additives of mineral oil results in a slight increase in viscosity at 40 °C, but no significant change can be seen at 100 °C. However, there was a significant increase in the flash point and fire point in case of the additivated samples as compared to the base MO.

Table 1. Physico-chemical properties of the lubricant samples.

Lubricant Samples	Viscosity at 40 °C (cSt)	Viscosity at 100 °C (cSt)	Flash Point (°C)	Fire Point (°C)
	(ASTM D 7279)	(ASTM D 7279)	(ASTM D 92)	(ASTM D 93)
MO	206	13.91	212	236
MO + 0.1% WS_2	207	14.61	240	251
MO + 0.5% WS_2	218	14.76	260	272
MO + 1.0% WS_2	218	14.56	260	272
MO + 2.0% WS_2	221	14.46	260	274
MO + 3.0% WS_2	222	14.36	265	276
MO + 4.0% WS_2	223	14.16	265	276
MO + 5.0% WS_2	223	14.59	275	285

Table 1. *Cont.*

Lubricant Samples	Viscosity at 40 °C (cSt)	Viscosity at 100 °C (cSt)	Flash Point (°C)	Fire Point (°C)
	(ASTM D 7279)	(ASTM D 7279)	(ASTM D 92)	(ASTM D 93)
MO + 0.1% PT	211	14.99	245	256
MO + 0.5% PT	224	14.98	255	267
MO + 1.0% PT	225	14.61	260	266
MO + 2.0% PT	224	14.55	265	278
MO + 3.0% PT	226	14.61	269	274
MO + 4.0% PT	227	14,46	270	283
MO + 5.0% PT	229	14.70	273	286
MO + 0.1% MoS_2	218	14.76	240	252
MO + 0.5% MoS_2	218	14.61	250	261
MO + 1.0% MoS_2	220	14.70	250	261
MO + 2.0% MoS_2	223	14.70	250	263
MO + 3.0% MoS_2	224	14.70	253	266
MO + 4.0% MoS_2	224	14.79	255	267
MO + 5.0% MoS_2	226	14.81	265	277

3. Results and Discussions

3.1. Analysing the Anti-Wear and Extreme Pressure Properties of the Oil Samples

The anti-wear tests were conducted according to the ASTM 4172 standards. Each test was repeated thrice in identical testing conditions. The wear scar diameters of the lower stationary balls were measured using the WINDUCOM image acquisition system (Make: DUCOM, Bengaluru, India). Figure 3 shows the average coefficient of friction (CoF) and the wear scar diameter (WSD). From Figure 3a it was observed that the CoF of some of the additivated oil samples was less than MO, while some of them exhibited a higher CoF than MO. The samples containing 3% PT, 3% MoS_2, and 2% WS_2 exhibited less CoF than MO. Among all the oil samples, 2% WS_2 exhibited the least CoF, followed by 3% PT and 3% MoS_2. The CoF of 2% WS_2 was about 37% less than MO, while CoF exhibited by 3% PT and 3% MoS_2 was 15.7% and 12.5% less than MO. Additionally, it was seen that 2% WS_2 exhibited 28% and 25% less CoF than 3% MoS_2 and 2% PT, respectively.

The wear scar diameter exhibited by the oil samples is shown in Figure 3b. It was seen that 3% PT exhibited the lowest WSD among all the oil samples. The WSD in case of 3% PT was about 12% less than MO. An amount of 0.1% MoS_2 showed the least WSD among the samples containing MoS_2 and 0.5% WS_2 showed the least WSD among the samples containing WS_2, but the WSD of MO without any additives was less than the WSDs of both 0.1% MoS_2 and 0.5% WS_2. The WSD of 3% PT was 12% and 10% less than of 0.1% MoS_2 and 0.5% WS_2-dispersed samples, respectively. Figure 4 shows images of the wear scars of the lower balls in the presence of various lubricants. Grooves and fine cracks were observed on balls tested using MO without any additives (Figure 4a). Grooves and sharp edged pits were also formed on the balls where WS_2 (Figure 4b) as well as MoS_2 (Figure 4c) were used as additives; however, the surface of the balls in presence of PT-dispersed MO (Figure 4d) exhibited minimal surface damage. This aspect indicates that there is a stable fluid film in case of PT-dispersed MO, which prevented metal–metal interaction, resulting in relatively lesser damaged surfaces in PT-dispersed MO as compared to MO without additives, MO with WS_2, and MoS_2.

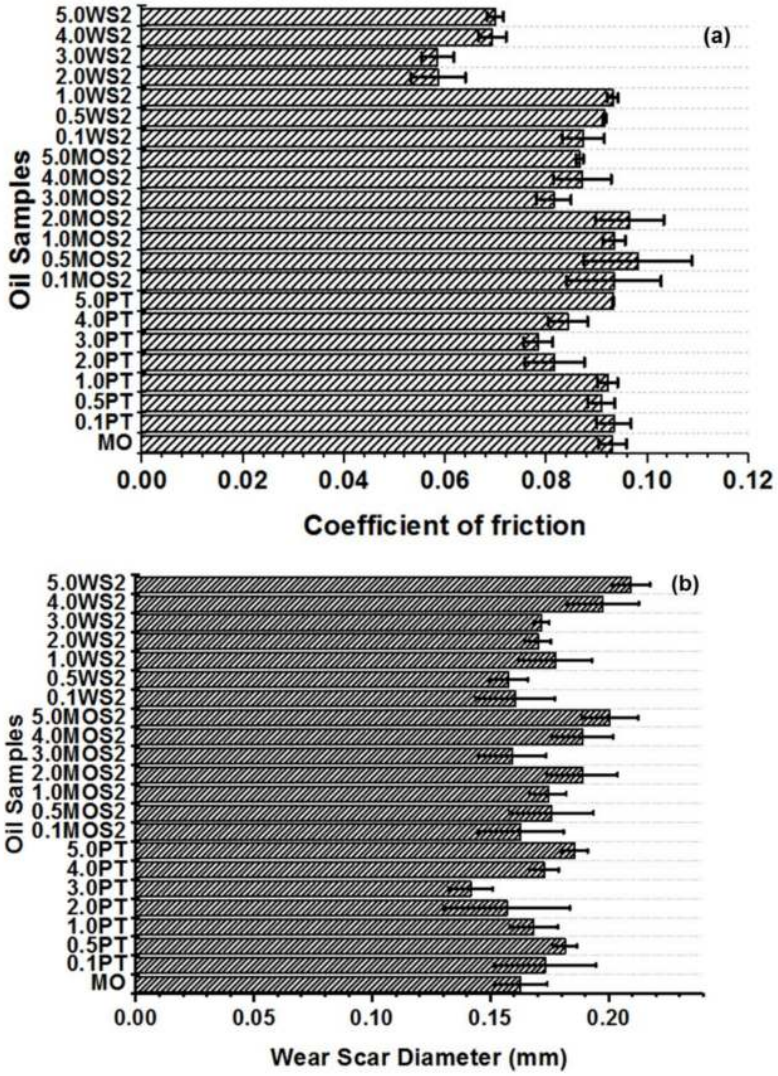

Figure 3. Anti-wear test results of oil samples. (**a**) Coefficient of friction; (**b**) Wear scar diameter (WSD).

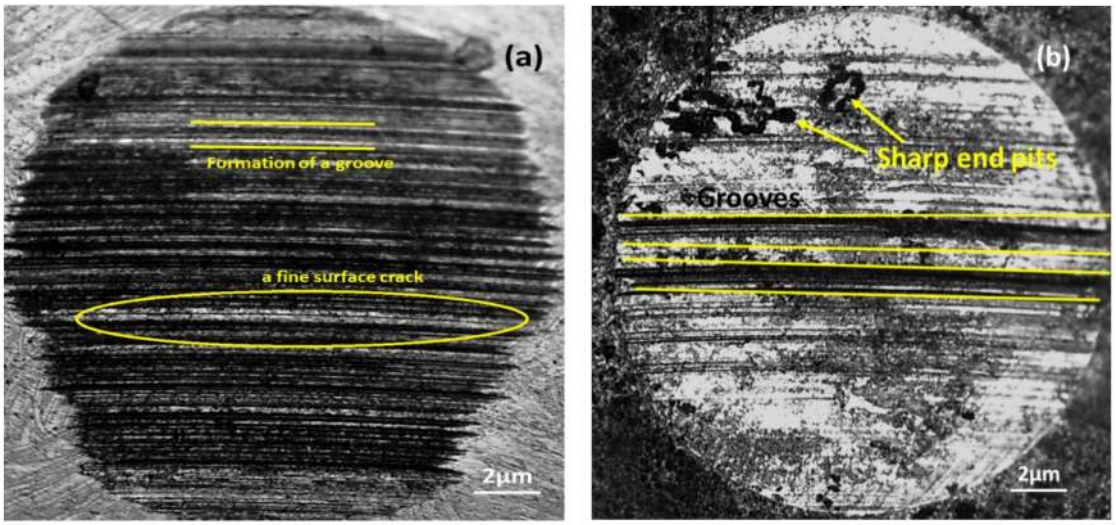

Figure 4. *Cont*.

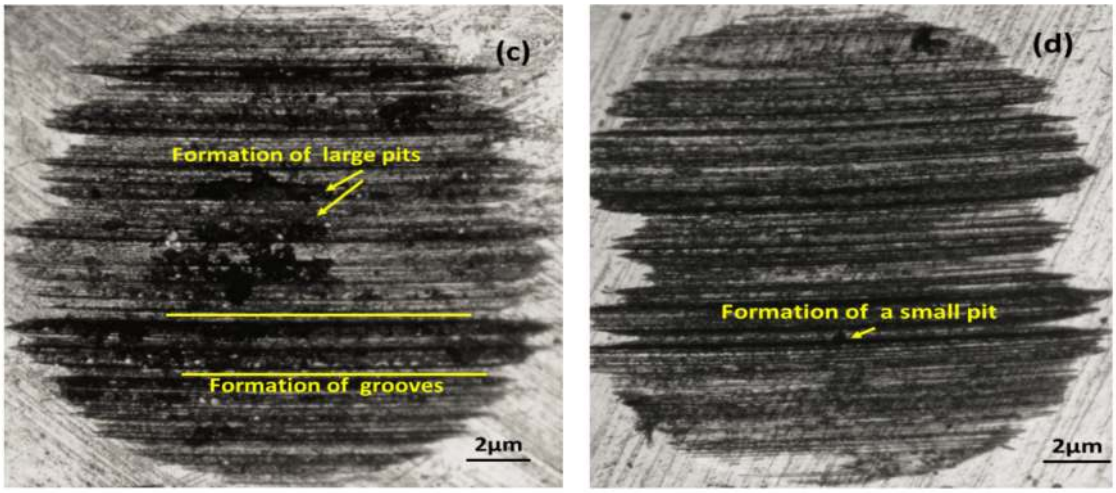

Figure 4. Optical microscopy pictographs of the wear scars on the balls with (**a**) MO, (**b**) 2% WS_2, (**c**) 3% MoS_2 and (**d**) 3% PT.

3.2. Analysing the Extreme Pressure Properties of the Oil Samples

The extreme pressure properties of the oil samples with the least COF were analysed according to ASTM 2783. From Figure 5, it was seen that the WSD of the oil samples containing 3% PT, 3% MoS_2 and 2% WS_2 were almost the same at 500 N and 630 N, but at 800 N, 1000 N and 1260 N the WSD of PT-dispersed oil samples was slightly higher than of MOS_2 and WS_2 samples; however, MO-lubricated samples were welded at 1600 N, but it is to be noted that the additivated MO samples exhibited better EP properties than the base MO without additives. The WSD of MO was larger than all the additivated samples at all loads, indicating that the EP properties enhanced with the addition of PT, MoS_2 and WS_2. Further to that, MO reached its weld load at 1260 N but the additivated samples did not weld, which further formed a strong point of enhanced EP properties of MO in the presence of PT, MoS_2 and WS_2. In fact, in the case of Figure 5e, the wear scar for the MO is the highest, as the welding generated circular wear traces on the tested balls and engaged in circular movement, even the three stationary balls from the pot.

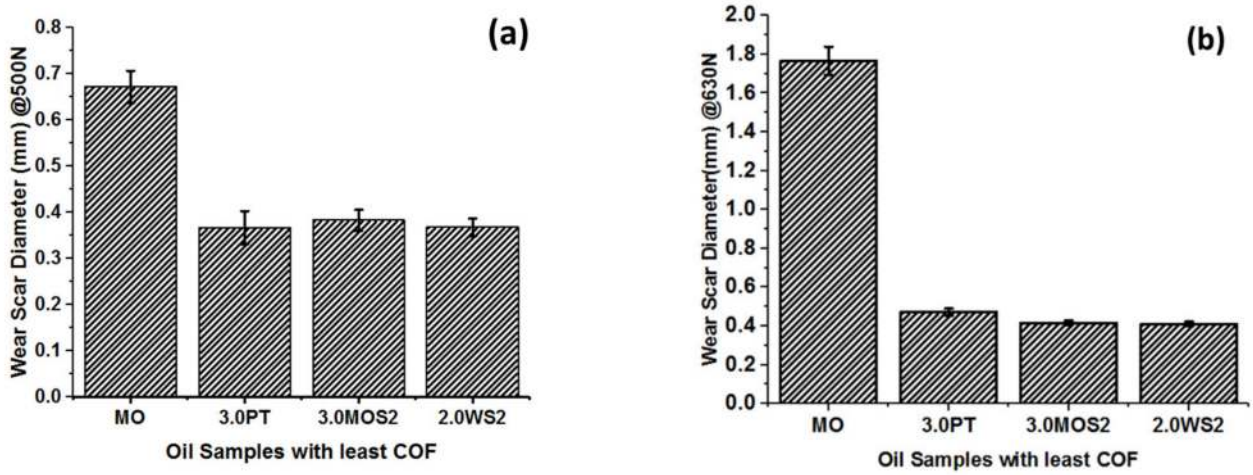

Figure 5. *Cont.*

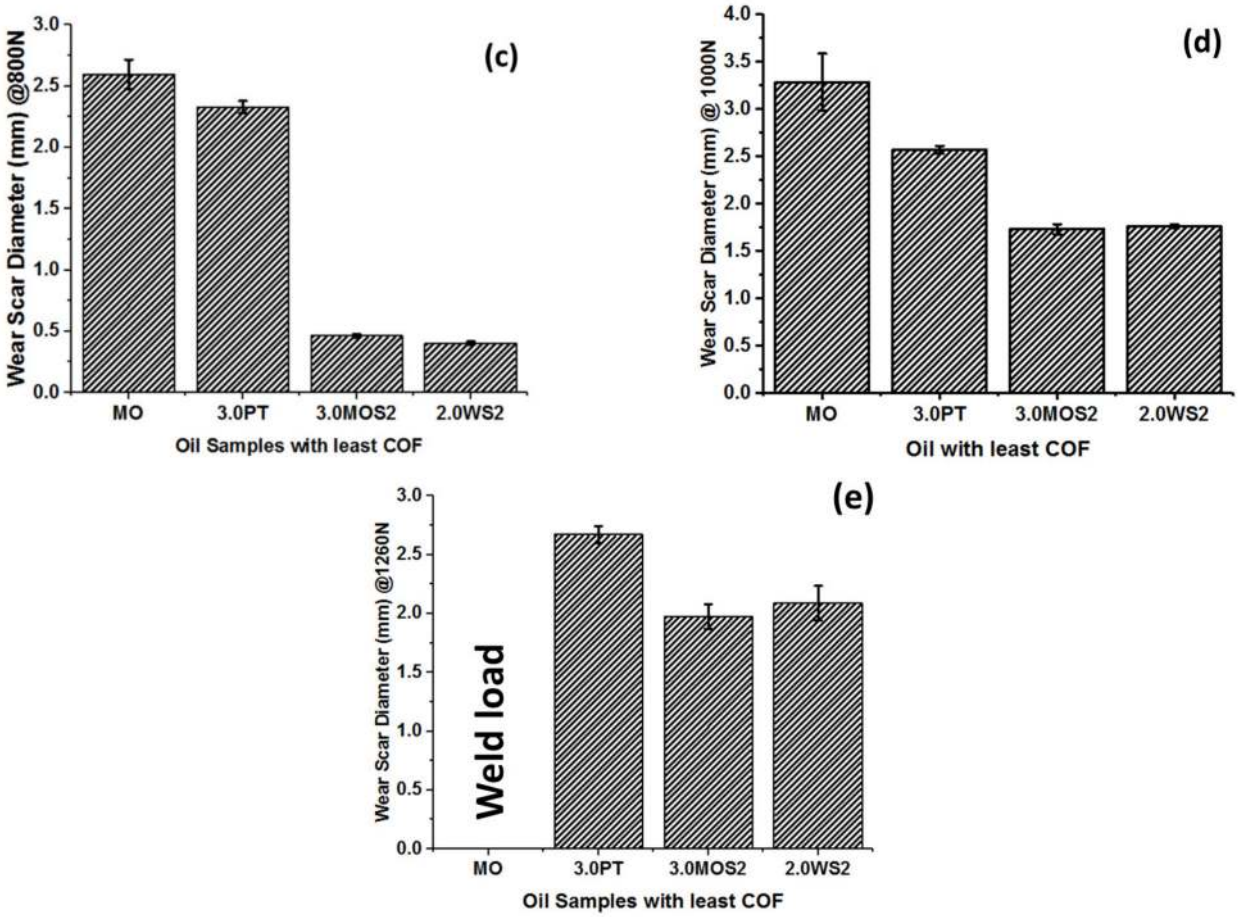

Figure 5. Wear scar diameters of the lubricant samples during extreme pressure tests at various loads of (**a**) 500 N, (**b**) 630 N, (**c**) 800 N, (**d**) 1000 N and (**e**) 1260 N.

3.3. Determining the Surface Roughness of the Balls and Iron Content of the Tested Oil

The surface roughness of the balls was measured using a non-contact 3D profilometer (Model: Talysurf CCI; Manufacturer: Taylor Hobson, Leicester, UK). The results of the roughness measurements are presented in Table 2. In order to further investigate the wear severity, the iron content in the oils after the anti-wear test were also determined as shown in Table 2. The iron content was determined using the ferrography method, according to ASTM D5185.

Table 2. The surface roughness of the balls and the Fe content in the oils after the anti-wear test.

Oil Samples	Ra (μm)	Rq (μm)	Fe Content (ppm)
Before test	0.146 ± 0.032	0.211 ± 0.046	0
MO	1.599 ± 0.094	3.624 ± 0.153	22.1
MO + 3% PT	1.213 ± 0.075	2.049 ± 0.116	20.0
MO + 3% MOS2	1.004 ± 0.063	1.650 ± 0.102	16.8
MO + 2% WS2	0.712 ± 0.047	1.582 ±0.098	4.56

The initial mean Ra roughness of the tested balls was 0.146 μm. The roughness of the balls tested with MO was higher than that corresponding to the balls tested in the presence of the additivated oil, indicating intense metal–metal contact between the balls lubricated with MO. For the additivated samples, the roughness was less than in the case of base MO, paving a point of better lubricating film. The better film stability in the additivated oil samples was further supported by the lesser amount of iron particles (Fe content) in

the additivated oil samples than MO. Among the additivated oil samples, WS_2-dispersed samples indicated a lower Fe content than PT and MoS_2-additivated oil samples.

The information regarding the measured roughness over the worn surfaces of the tested balls must be correlated with optical microscopy images and Raman spectroscopy results. In addition, the results regarding the variation of the friction coefficient correlated with the wear scar diameter measurements, offering a good insight on the entire wear mechanism.

3.4. Investigating the Rolling Contact Fatigue Resistance of AISI 52100 Balls in Presence of the Lubricants

RCF is one of the key factors in component failure in turbomachinery, which includes bearings, gears, cam followers, etc. RCF occurs when alternating the developed stress in a small volume of material, as in non-conformal contacts of the rolling elements. In case of meshing of the gear teeth, the motion involved is rolling–sliding. Thus, apart from protecting from sliding wear, a gear lubricant must also have a good rolling fatigue resistance. In RCF, microcracks may occur due to local discontinuities, becoming macrocracks that propagate to the surface, and ultimately resulting in the removal of a piece of material from the surface and the creation of pitting/spalling. RCF in lubricated contacts is generally characterized as pitting and micro-pitting, depending on the size of the pits. Micro-pitting is particularly common on ground steel surfaces and is generally attributed to the stress field associated with the roughness of the contact surfaces.

The rolling contact behaviour of the bearing balls in the presence of the oil samples was investigated using the four-ball tribometer, and the data were analysed using the Weibull plot and survival probability curves [20]. Weibull is an effective method to statistically predict the life span of the contact. The L_{10}, L_{50} and L_{90} lives represent the reliabilities of a machine element subjected to cyclic stress, for 90%, 50%, and 10% of survivability probability. To determine these values, tests must be carried out sequentially increasing the stress acting on the considered machine element; in our case, the increasing axial load generating increased normal and tangential stresses between the tested balls.

Assuming a Weibull distribution of failures, the equation describing the reliability is:

$$R(t) = exp\left(-\frac{x}{\alpha}\right)^{\beta} \quad (1)$$

where x represents the number of cycles (time) till failure, α is the characteristic life parameter or scale parameter which offers information about the spread in the data distribution and β is the shape parameter (Table 3). A high shape parameter indicates an increased failure rate. From Table 3, it can be seen that WS_2-dispersed MO has the highest shape parameter (β = 4.0316), followed by MO without any additives (β = 3.0421). PT-dispersed MO exhibited a lower shape parameter (β = 2.6810) than MO and MO with WS_2. The lowest shape parameter among all the samples was exhibited by MoS_2-dispersed MO (β = 1.7730). Additionally, it was seen that the characteristic life of MO was enhanced by 70% when MOS_2 and PT were dispersed in MO. Figure 6 shows the Weibull plot of the oil samples.

Table 3. Weibull parameters for the oil samples.

Oil Samples	Shape Parameter (β)	Characteristic Life (α)
MO	3.0421	103,973
MO + 3% PT	2.6810	354,551
MO + 2% WS_2	4.0316	87,844
MO + 3% MOS_2	1.7730	349,494

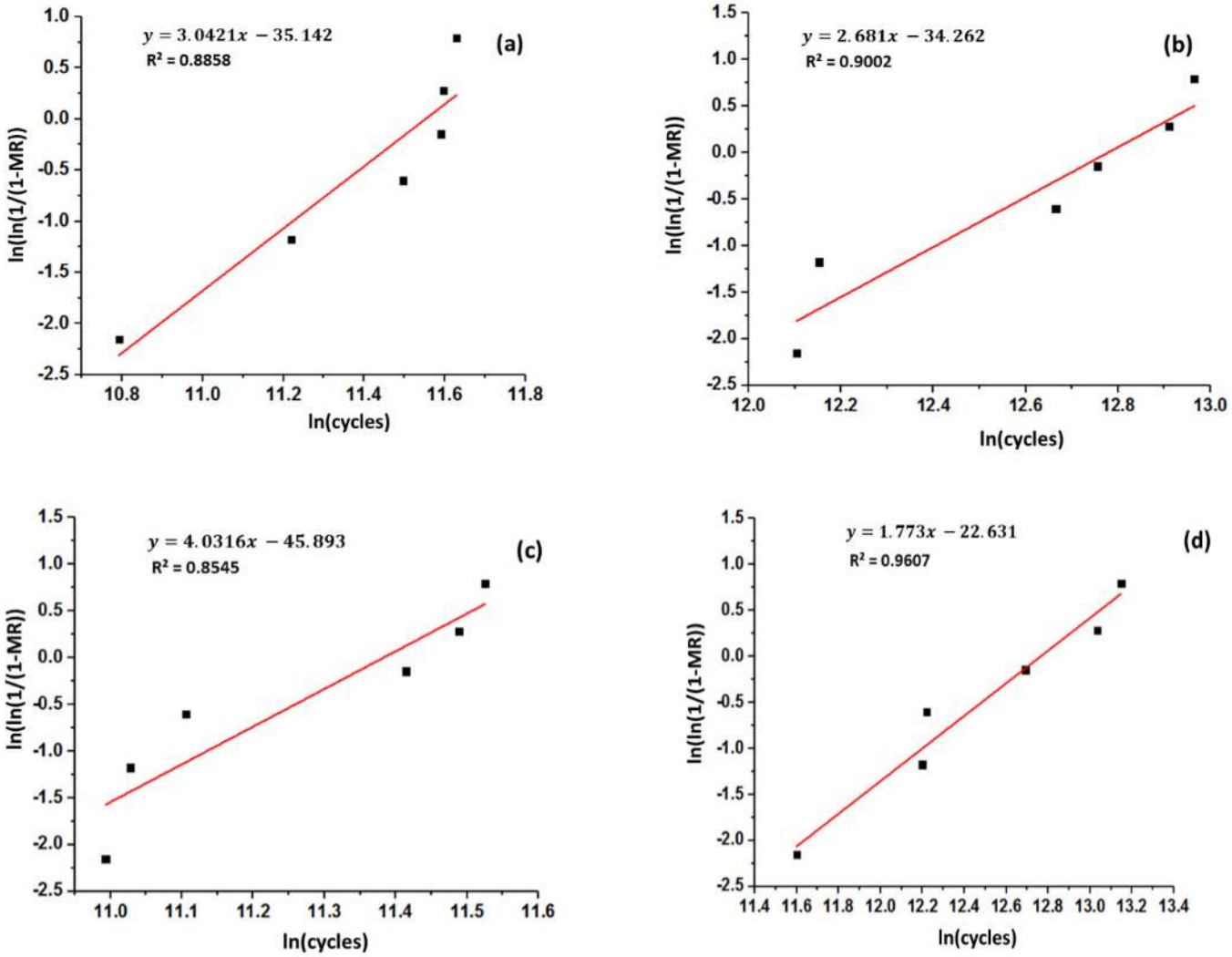

Figure 6. Weibull plots for (**a**) MO, (**b**) MO + PT, (**c**) MO + WS_2 and (**d**) MO+ MoS_2.

The survival probability curve is shown in Figure 7. It can be seen that MO containing PT and MoS_2 exhibited better survival probability compared to WS_2-dispersed MO and MO without any additives. It is to be noted that even though MoS_2 initially showed a higher survival probability than PT-dispersed MO, at about 388,000 cycles the situation changed, and PT exhibited a better survival probability than MoS_2. Furthermore, it was observed that the L_{10}, L_{50} and L_{90} life of MoS_2 and PT-dispersed MO were higher than the MO and WS_2-dispersed MO, indicating that usage of MoS_2 and PT enhanced the rolling contact fatigue life of the bearing balls, an important role being played by the lubricant.

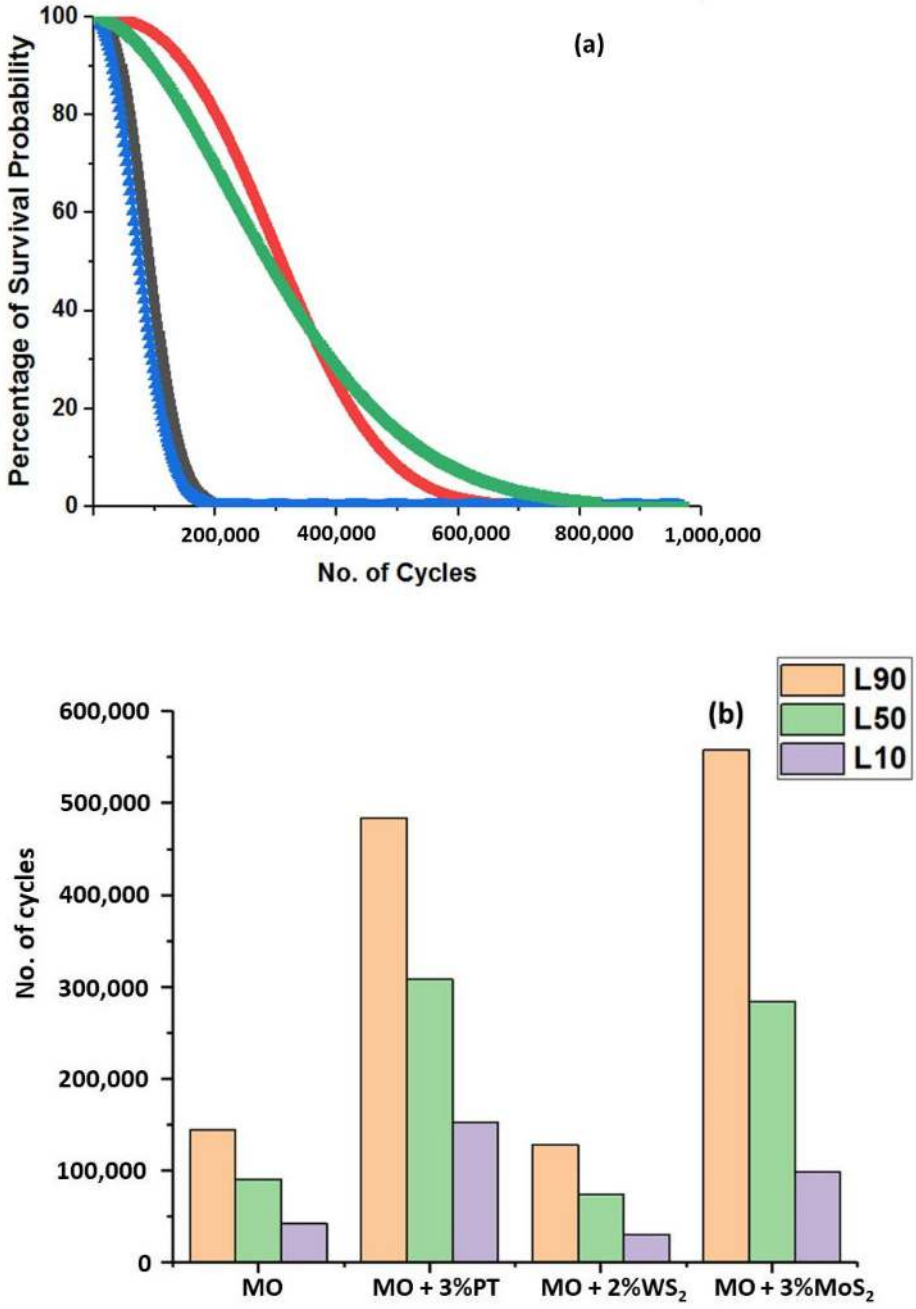

Figure 7. (**a**) Percentage of survival probability; (**b**) Life cycles in presence of lubricants with and without additives.

4. Analysing the Surfaces After Tribo-Tests and the Tribo-Film between the Surfaces

In order to understand the formation of tribo-film during the anti-wear tests, the wear tracks were further analysed by optical microscopy. The formation of a stable protective layer on the wear tracks is responsible for enhancing the tribological properties of the lubricant; thus, increasing the fatigue life of the mechanical component (steel balls). The applied load and shear of the lubricant due to the rolling action during the RCF tests generated high local stresses at the contact points. The presence of a stable film between the tribo-pairs would prevent the contact between the two bodies. Any wear or crack formation on the surface is the result of the cyclic stresses due to the repeated rolling contacts. From Sections 3.1 and 3.2, it was seen that, even though the CoF in WS_2 was lowest, the balls in the presence of MO and WS_2-dispersed MO exhibited less RCF life than the balls in the

presence of PT and MoS_2-dispersed MO. The wear scar diameter of WS_2-dispersed MO was larger than PT-dispersed MO and slightly higher than MoS_2-dispersed MO, indicating the chances of film breakage on the steel surfaces. The breakage of film resulted in contact between the mating pairs, which initiated deep scratches, resulting in the formation of cracks. Figure 8 shows the optical microscope images of the balls after the RCF test. High amounts of pitting and surface cracks were observed on the ball surfaces where MO and WS_2-dispersed MO was used, indicating high contact between the mating surfaces. However, the pitting and surface cracks on the balls were found to be less in case of MoS_2 (Figure 8e,f) and PT-dispersed MO (Figure 8g,h), making a strong point of the presence of stable film in case of MoS_2 and PT-dispersed MO as compared to MO (without additives) and WS_2-dispersed MO. To the best of the knowledge of the authors, this observation of damaged surfaces during rolling contact fatigue has not been reported so far for the tested oil samples.

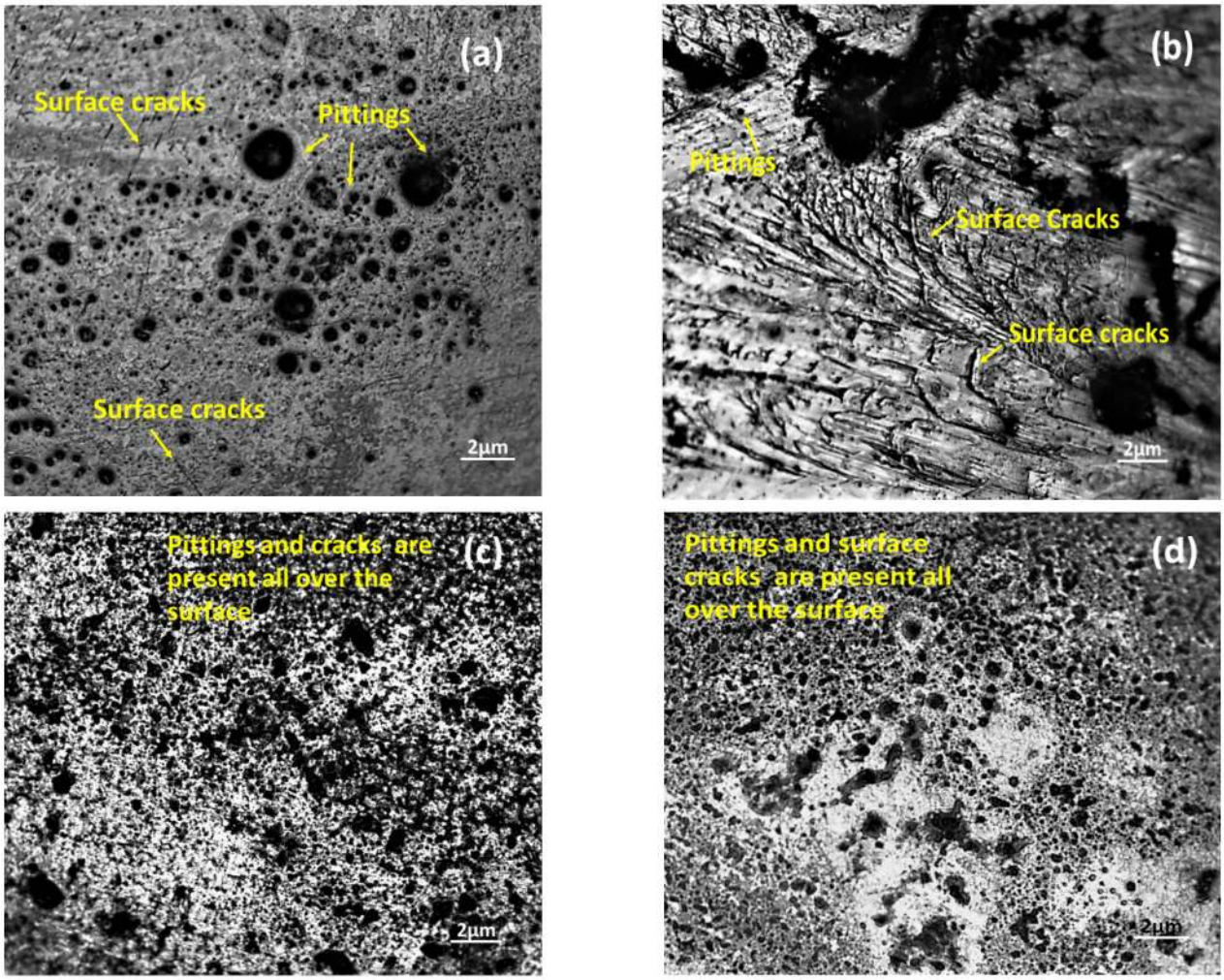

Figure 8. *Cont.*

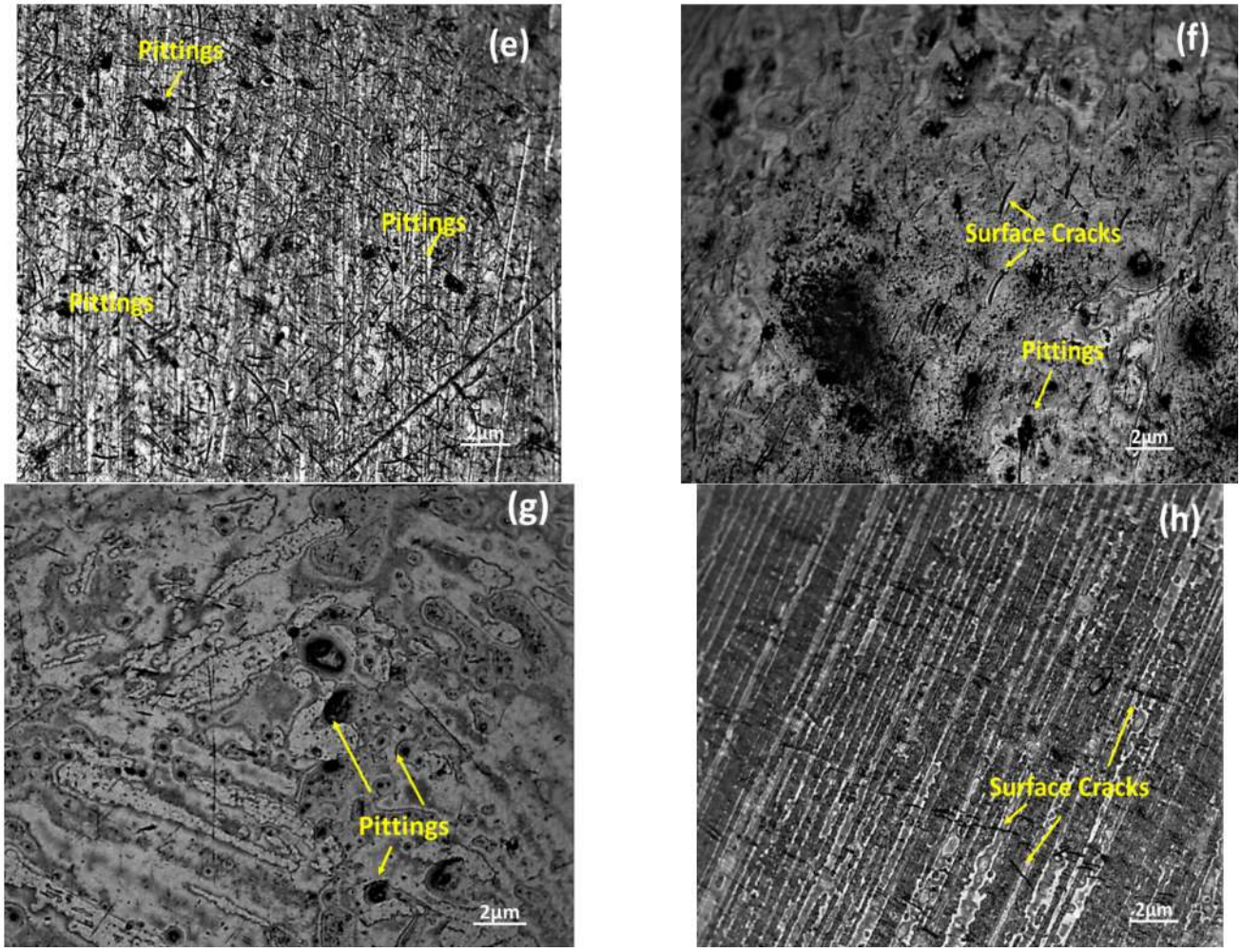

Figure 8. Optical microscope images of steel balls after rolling contact fatigue test: (**a**,**b**) MO; (**c**,**d**) MO + 2% WS_2; (**e**,**f**) MO + 3% MoS_2; (**g**,**h**) MO + 3% PT.

5. Discussion

In order to understand the lubrication mechanisms, the wear scars on the steel balls were analysed using a Raman spectrograph. The Raman spectroscopy was realized in the middle of each wear spot, where the effect of additive is obvious. We chose not to represent the corresponding points, as they unnecessarily masked the worn surface and the observations we noted on those figures regarding the wear modes.

Figure 1 presents Raman spectroscopy results of the employed additives alone, while Figure 9 presents Raman spectroscopy results of the wear scars on the balls after anti-wear tests. As can be observed, the results from Figure 9 confirm that the presence of the additives on the worn surfaces of the balls shows their effectiveness in slowing down the wear process of mating balls during the anti-wear tests. The Raman spectra indicated the deposition of the additives on the wear track, confirming the formation of a protective layer between the steel balls; thus, reducing the frictional coefficient. Highly damaged surfaces in case of MO and MO + 2% WS_2 indicated lubricating film breakage during the RCF tests. Looking into the Raman spectra of the wear scars, strong peaks of WS_2 were observed in Figure 9a, no other secondary peaks were detected in the Raman spectra, whereas in case of MoS_2 and PT—apart from the peaks of MoS_2 and PT—several other peaks were observed on the wear scar, indicating the presence of various layers of protective tribo-films, which prevented most of the direct contact between the mating surfaces, and restricted the formation of surface cracks on the ball surfaces lubricated with MoS_2 and PT-dispersed MO. The Raman spectra indicated that all the additives were able to form a tribo-film but WS_2,

the reported strong peaks (360 cm^{-1}, 430 cm^{-1}) being near to those of WS_2 peaks reported earlier [21]. The difference in the position of the peaks of WS_2 is due to the possibility of the presence of defects, which might have generated during the tribo-tests. Similar results of detection of only WS_2 without any other reactant products in the tribo-film was also reported by Wu et al. [22]. However, in case of MoS_2 and PT, apart from the deposition of the additives, several other peaks were also observed, especially iron oxides. The Raman spectra at 287 cm^{-1}, 360 cm^{-1}, 391 cm^{-1}, 416 cm^{-1} and 473 cm^{-1} are quite close to the Raman spectra of MoS_2 as reported by Tillman et al. [23], indicating the deposition of MoS_2 on the wear tracks. In addition, weak spectra of molybdenum oxides (MoO_2) was also detected at 744 cm^{-1} [24]. Apart from those peaks, there were sharp peaks at several places which were difficult to identify, indicating several tribo-chemical reactions at the contact points. In case of WS_2 the continuous rolling action of the balls may have caused the decomposition of WS_2 into WO_3, S and SO_4 which were easily detached from the surface of the wear scars; hence, on analysing the wear scars of balls, those were not detected for WS_2. A weak peak at 270.1 cm^{-1} indicates the possibility of oxides of tungsten [25]. Additionally, the quantity of such kind of decomposed elements would be less at temperature at which the test was conducted (ball pot temperature in the present work was 75 °C). However, a similar observation of breaking MoS_2 and WS_2 was reported by Wong et al. [26]. The reason why the coefficient of friction was low is the easy shearing of the oxide layer, exposing the parent material simultaneously which affected the surface during the RCF tests. The bottom balls impacted each other without any protective film between them, resulting in the generation of easy surface cracks and pitting.

The Raman spectra of the wear scars of the balls in the presence of PT presented several peaks, such as 680 cm^{-1}, 757 cm^{-1}, and 900 cm^{-1}; these values being quite close to those peaks of PT powder (Figure 1), indicating the deposition of PT on the surfaces of the mating pairs and the formation of a stable tribo-film. Thus, it can be inferred that the additive formed a stable film between the tribo-pairs. Apart from the stable lubricating film deposited on the tribo-pairs, the structures of the additives also contributed in controlling the friction between the tribo-pairs. In the present investigation, all three additives are 2D materials with layered structure, and sliding between these layers reduces the coefficient of friction. The reported values of interlayer spacing in case of MoS_2 and WS_2 are approximately 6.15–6.5 Å [27–29], while for PT the interlayer spacing is 15.532 Å [30]. The friction reduction in case of these lamellar additives is due to the weak van der Waals forces between the layers, which shear themselves easily; hence, the increase in the interlayer spacing will result in further easy shearing, making a strong point for an enhanced performance of PT than MoS_2 and WS_2; thus, reducing the friction between the tribo-pairs [22]. However, WS_2 indicated a lower coefficient of friction; this may be due to the stable film during the short anti-wear tests, but in the extended RCF tests, when the situation was more dynamic due to the free rotation of the lower balls (as the bottom balls are not fixed), the WS_2 could not form a stable film and resulted in the easy formation of surface cracks.

Regarding the wear modes of the AISI 52100 balls subjected to the anti-wear tests, it can be observed that there are many surface cracks and pits obtained for the non-additivated mineral oil (Figure 8a,b). For the MO + 2% WS_2 samples (Figure 8c,d), only numerous pits can be observed, the additive hindering the formation of cracks due to the reason previously presented—the presence of lamellar additive between the mating surfaces. The brittle structure of MoS_2, which also possesses a layered structure in which the stacked monolayers are held together by weak van der Waals interactions, conducted to the formation of both pits and micro-cracks as—from place to place—direct contact between the metals occurred (Figure 8e,f). The most protective action against wear is reported for the MO + 3% PT, the layered structure of PT, composed by flakes and sheet-like shapes, being more resistant to shearing in tribological contacts (Figure 8g,h).

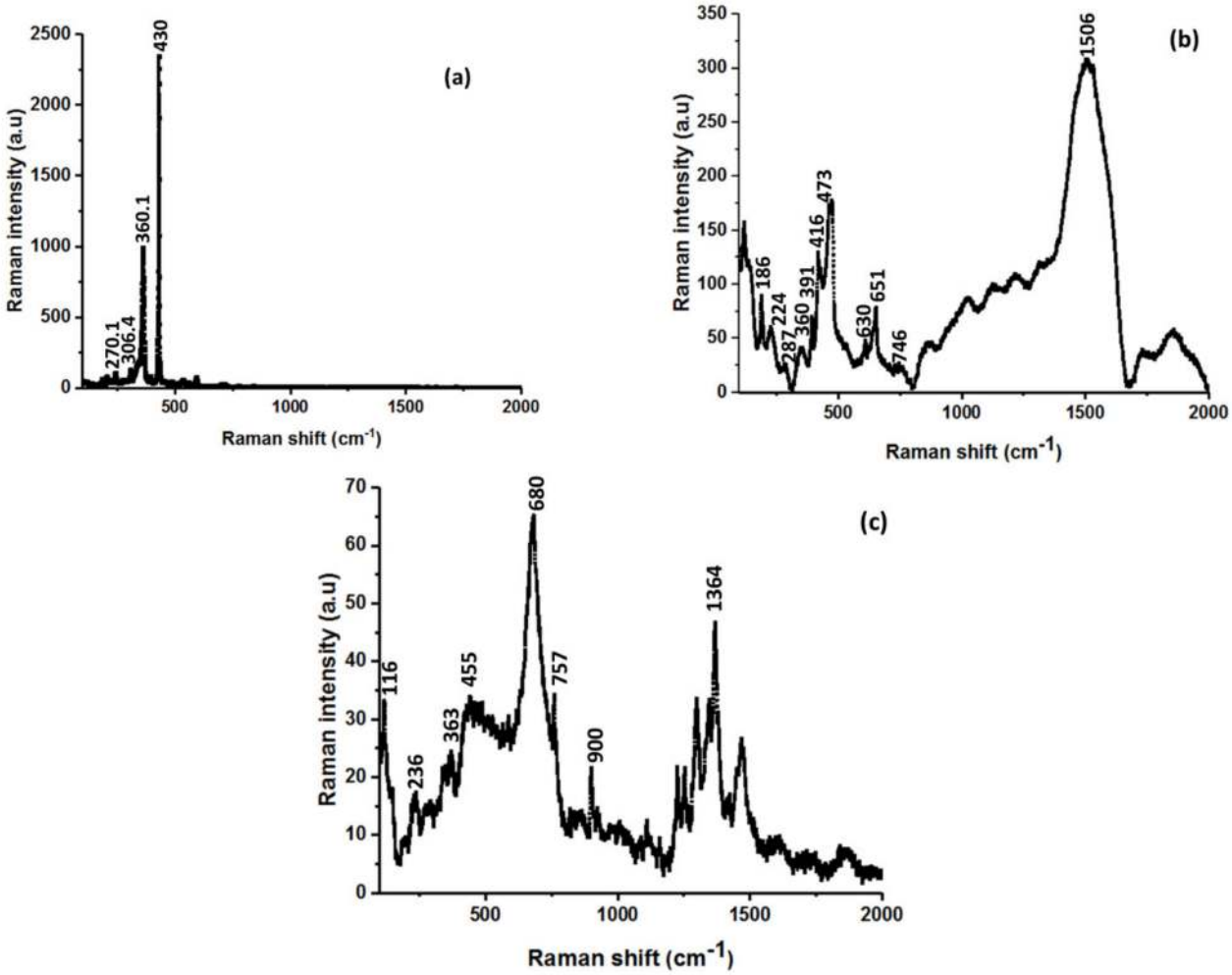

Figure 9. The Raman spectra of the wear scars on the stationary balls after the anti-wear tests. (**a**) WS_2-dispersed MO; (**b**) MoS_2-dispersed MO; (**c**) PT-dispersed MO.

6. Conclusions

The present work investigated the tribological properties of tungsten disulphide, molybdenum disulphide and lithium potassium titanate-added mineral oil using a four-ball tribometer. At the end of the anti-wear tests, it was observed that 3 wt.% PT and MoS_2 and 2% WS_2 exhibited a lower coefficient of friction among other concentrations. Though WS_2-added mineral oil exhibited the lowest frictional coefficient, the wear scar on the steel balls in case of PT-added mineral oil was the smallest, followed by MoS_2-added mineral oil. The optical microscopic images of the wear scars on the balls in case of PT-added mineral oil did not exhibit major surface damages as compared to the other lubricants. During the extreme pressure tests, it was seen that PT presented comparable wear scars with MoS_2 and WS_2 additives, indicating similar extreme pressure properties of the additivated lubricants. The mineral oil without any additives welded at 1260 N; however, no welding of the additivated lubricants was observed at 1260 N, indicating an enhancement in the extreme pressure properties with the addition of all the additives. Furthermore, during the extended rolling contact fatigue tests, PT-added mineral oil exhibited the highest life cycles, followed by MoS_2 and WS_2-added mineral oil; thus, indicating PT to be a plausible alternative to MoS_2 and WS_2. Thus, it can be concluded that with the addition of appropriate additives in mineral oil, the life of bearing steel AISI 52100 can be enhanced.

Author Contributions: Conceptualization, S.B. and V.P.; methodology, S.B. and V.P.; software, S.B. and V.P.; validation, S.B. and V.P.; formal analysis, S.B. and V.P.; investigation, S.B. and V.P.; resources, S.B.; data curation, S.B. and V.P.; writing—original draft preparation, S.B. and V.P.; writing—review and editing, V.P.; visualization, S.B. and V.P.; supervision, S.B. and V.P.; project administration, S.B.; funding acquisition, S.B. All authors have read and agreed to the published version of the manuscript.

Funding: This research received no external funding.

Informed Consent Statement: Informed consent was obtained from all subjects involved in the study.

Acknowledgments: The author acknowledges the support of Alroko GmbH & Co KG, Germany (www.alroko.de) and Otsuka Chemical Co., Ltd., Japan (www.otsukac.co.jp) for supplying the additives (lithium potassium titanate, molybdenum disulphide and tungsten disulphide).

Conflicts of Interest: The authors declare no conflict of interest.

References

1. Omrani, E.; Menezes, P.L.; Rohatgi, P.K. Effect of Micro- and Nano-Sized Carbonous Solid Lubricants as Oil Additives in Nanofluid on Tribological Properties. *Lubricants* **2019**, *7*, 25. [CrossRef]
2. Bhaumik, S.; Paleu, V.; Pathak, R.; Maggirwar, R.; Katiyar, J.K.; Sharma, A.K. Tribological investigation of r-GO additived biodegradable cashew nut shells liquid as an alternative industry lubricant. *Tribol. Int.* **2019**, *135*, 500–509. [CrossRef]
3. Jiang, F.; Sun, H.; Chen, L.; Lei, F.; Sun, D. Dispersion–tribological property relationship in mineral oils containing 2D layered α-zirconium phosphate nanoplatelets. *Friction* **2020**, *8*, 695–707. [CrossRef]
4. Fayaz, S.D.; Wani, M.F. Insights into the tribological behavior of IF-WS2 nanoparticle reinforced mild extreme pressure lubrication for coated chromium/bulk grey cast iron interface. *Proc. Inst. Mech. Part J.* **2020**, *7*. [CrossRef]
5. Bhowmick, S.; Eskandari, B.; Krishnamurthy, G.; Alpas, A.T. Effect of WS2 particles in cutting fluid on tribological behaviour of Ti–6Al–4V and on its machining performance. *Tribol. Mater. Surf. Interf.* **2020**. [CrossRef]
6. Yan, C.; Zeng, Q.; Hao, Y.; Xu, Y.; Zhou, M. Friction-Induced Hardening Behaviors and Tribological Properties of 60NiTi Alloy Lubricated by Lithium Grease Containing Nano-BN and MoS2. *Tribol. Trans.* **2019**, *62*, 812–820. [CrossRef]
7. Song, W.; Yan, J.; Ji, H. Fabrication of GNS/MoS2 composite with different morphology and its tribological performance as a lubricant additive. *Appl. Surf. Sci.* **2019**, *469*, 226–235. [CrossRef]
8. Charoo, M.S.; Wani, M.F.; Hanief, M.; Rather, M.A. Tribological Properties of MoS2 Particles as Lubricant Additive on EN31 Alloy Steel and AISI 52100 Steel Ball. *Mater. Today Proc.* **2017**, *4*, 9967–9971. [CrossRef]
9. Saidi, M.Z.; Pasc, A.; Moujahid El, C.; Canilho, N.; Badawi, M.; DelgadoSanchez, C.; Celzard, A.; Fierro, V.; Peignier, R.; Kouitat-Njiwa, R.; et al. Improved tribological properties, thermal and colloidal stability of poly-α-olefins based lubricants with hydrophobic MoS2 submicron additives, *J. Colloid Interf. Sci.* **2020**, *562*, 91–101. [CrossRef]
10. Akbulut, M. Nanoparticle-based lubrication systems. *J. Powder Metall Min* **2012**, *1*. [CrossRef]
11. Hu, K.H.; Hu, X.G.; Xu, Y.F.; Huang, F.; Liu, J.S. The effect of morphology on the tribological properties of MoS2 in liquid paraffin. *Tribol. Lett.* **2010**, *40*, 155–165. [CrossRef]
12. Vaitkunaite, G.; Espejo, C.; Wang, C.; Thiebaut, B.; Charrin, C.; Neville, A.; Morina, A. MOS2 tribofilm distribution from low viscosity lubricants and its effect on friction. *Tribol. Int.* **2020**, *151*, 106531. [CrossRef]
13. An, V.; Irtegov, Y.; De Izarra, V. Study of Tribological Properties of Nanolamellar WS2 and MoS2 as Additives to Lubricants. *J. Nanomaterials* **2014**, 865839. [CrossRef]
14. Berkdemir, A.; Gutiérrez, H.R.; Botello-Méndez, A.R.; Perea-López, N.; Elías, A.L.; Chia, C.I.; Wang, B.; Crespi, V.H.; López-Urías, F.; Charlier, J.C.; et al. Identification of individual and few layers of WS2 using Raman Spectroscopy. *Sci. Rep.* **2013**, *3*, 1755. [CrossRef]
15. Najmaei, S.; Liu, Z.; Ajayan, P.M.; Lou, J. Thermal effects on the characteristic Raman spectrum of molybdenum disulfide (MoS2) of varying thicknesses. *Appl. Phys. Lett.* **2012**, *100*, 013106. [CrossRef]
16. Wang, Q.; Guo, Z.; Chung, J.S. Formation and structural characterization of potassium titanates and the potassium ion exchange property. *Mater. Res. Bull.* **2009**, *44*, 1973–1977. [CrossRef]
17. Lee, S.Y.; Lee, C.H.; Kim, D.Y.; Locquet, J.; Seo, J.W. Preparation and Photocatalytic Activity of PotassiumIncorporated Titanium Oxide Nanostructures Produced by the Wet Corrosion Process Using Various Titanium Alloys. *Nanomaterials* **2015**, *5*, 1397–1417. [CrossRef] [PubMed]
18. Bhaumik, S.; Kamaraj, M.; Paleu, V. Tribological analyses of a new optimized gearbox biodegradable lubricant blended with reduced graphene oxide nanoparticles. *Proc. Inst. Mech. Part J.* **2020**. [CrossRef]
19. Bhaumik, S.; Paleu, V.; Sharma, S.; Dwivedi, S.; Borkar, S.; Kamaraj, M. Nano and micro additivated glycerol as a promising alternative to existing non-biodegradable and skin unfriendly synthetic cutting fluids. *J. Cleaner Prod.* **2020**, *263*, 121383. [CrossRef]
20. Thapliyal, P.; Thakre, G.D. Influence of Cu nanofluids on the rolling contact fatigue life of bearing steel. *Eng. Fail. Anal.* **2017**, *78*, 110–121. [CrossRef]
21. Mishra, A.K.; Lakshmi, K.V.; Huang, L. Eco-friendly synthesis of metal dichalcogenides nanosheets and their environmental remediation potential driven by visible light. *Sci. Rep.* **2015**, *5*, 15718. [CrossRef] [PubMed]

22. Wu, N.; Hu, N.; Wu, J.; Zhou, G. Tribology Properties of Synthesized Multiscale Lamellar WS2 and Their Synergistic Effect with Anti-Wear Agent ZDDP. *Appl. Sci.* **2020**, *10*, 115. [CrossRef]
23. Tillmann, W.; Wittig, A.; Stangier, D.; Thomann, C.-A.; Moldenhauer, H.; Debus, J.; Aurich, D.; Brümmer, A. Investigation of the Tribofilm Formation of HiPIMS Sputtered MoSx Thin Films in Different Environments by Raman Scattering. *Lubricants* **2019**, *7*, 100. [CrossRef]
24. Dieterle, M.; Mestl, G. Raman spectroscopy of molybdenum oxides. Part II. Resonance Raman spectroscopic characterization of the molybdenum oxides Mo_4O_{11} and MoO_2. *Phys. Chem. Chem. Phys.* **2002**, *4*, 822–826. [CrossRef]
25. Djaoued, Y.; Balaji, S.; Bruning, R. Electrochromic devices based on porous tungsten oxide thin films. *J. Nanomater.* **2012**, 674168. [CrossRef]
26. Wong, K.C.; Lu, X.; Cotter, J.; Eadie, D.T.; Wong, P.C.; Mitchell, K.A.R. Surface and friction characterization of MoS2 and WS2 third body thin films under simulated wheel/rail rolling–sliding contact. *Wear* **2008**, *264*, 526–534. [CrossRef]
27. Sun, J.; Li, X.; Guo, W.; Zhao, M.; Fan, X.; Dong, Y.; Xu, C.; Deng, J.; Fu, Y. Synthesis Methods of Two-Dimensional MoS2: A Brief Review. *Crystals* **2017**, *7*, 198. [CrossRef]
28. Wu, J.-Y.; Lin, M.-N.; Wang, L.-D.; Zhang, T. Photoluminescence of MoS2 Prepared by Effective Grinding-Assisted Sonication Exfoliation. *J. Nanomaterials* **2014**, *2014*, 852735. [CrossRef]
29. Xu, J.; Zhang, J.; Zhang, W.; Shin Lee, C. Interlayer Nanoarchitectonics of Two-Dimensional Transition-Metal Dichalcogenides Nanosheets for Energy Storage and Conversion Applications. *Adv. Energy Mater.* **2017**, *7*, 1700571. [CrossRef]
30. Sasaki, T.; Kooli, F.; Iida, M.; Michiue, Y.; Takenouchi, S.; Yajima, Y.; Izumi, F.; Chakoumakos, B.C.; Wanabe, M. A Mixed Alkali Metal Titanate with the Lepidocrocite-like Layered Structure. Preparation, Crystal Structure, Protonic Form, and Acid−Base Intercalation Properties. *Chem. Mater.* **1998**, *10.12*, 4123–4128. [CrossRef]